ALMA MATER STUDIORUM
UNIVERSITÀ DI BOLOGNA

ARCHIVIO ISTITUZIONALE
DELLA RICERCA

Alma Mater Studiorum Università di Bologna
Archivio istituzionale della ricerca

Insights into PLGA-encapsulated epigallocatechin 3-gallate nanoparticles as a new potential biomedical system: A computational and experimental approach

This is the final peer-reviewed author's accepted manuscript (postprint) of the following publication:

Published Version:
Minnelli, C., Stipa, P., Sabbatini, S., Mengucci, P., Mobbili, G., Galeazzi, R., et al. (2023). Insights into PLGA-encapsulated epigallocatechin 3-gallate nanoparticles as a new potential biomedical system: A computational and experimental approach. EUROPEAN POLYMER JOURNAL, 182, 1-11 [10.1016/j.eurpolymj.2022.111723].

Availability:
This version is available at: https://hdl.handle.net/11585/919251 since: 2025-01-23

Published:

DOI: http://doi.org/10.1016/j.eurpolymj.2022.111723

Terms of use:

Some rights reserved. The terms and conditions for the reuse of this version of the manuscript are specified in the publishing policy. For all terms of use and more information see the publisher's website.

This item was downloaded from IRIS Università di Bologna (https://cris.unibo.it/).
When citing, please refer to the published version.

(Article begins on next page)

20 February 2025

Insights into PLGA-Encapsulated Epigallocatechin 3-Gallate nanoparticles as a new potential biomedical system: a computational and experimental approach

Cristina Minnelli[b], Pierluigi Stipa[a], Simona Sabbatini[a], Paolo Mengucci[a], Giovanna Mobbili[b], Roberta Galeazzi[b], Tatiana Armeni[c], Brenda Romaldi[c], Annamaria Celli[d], Emiliano Laudadio[a]*

Corresponding author

Email address: e.laudadio@staff.univpm.it (E. Laudadio)

a Department of Materials, Environmental Sciences and Urban Planning, Polytechnic University of Marche, Ancona, Italy;

b Department of Life and Environmental Science, Polytechnic University of Marche, Ancona, Italy;

c Department of Clinical Sciences, Polytechnic University of Marche, Ancona, Italy;

d Department of Civil, Chemical, Environmental and Materials Engineering, Bologna, Italy

Abstract: Biodegradable poly-lactic poly-glycolic copolymer (PLGA) represents one of the best strategies adopted to convey small molecules unstable and characterised by a low bioavailability if administered without vehicles. This is the case of Epigallocatechin-3-gallate (EGCG), which is one of the most interesting polyphenols from a biomedical point of view. In this study, the impact of EGCG on PLGA nanoparticles (NPs) properties has been studied underlining the role of the binary PVA/Poloxamer-407 as stabilizer system for obtaining colloidal stable NPs. Characterization has been carried out by dynamic light scattering (DLS), encapsulation efficiency, drug release studies, scanning electron microscopy (SEM) and infrared spectroscopy (IR). Molecular dynamics (MD) simulations have been used to model the PLGA and EGCG systems to understand the behaviour of NPs and the interactions that guided the EGCG encapsulation. The nanodispersions exhibited promising cytotoxic potentials in human lung carcinoma A549 cell lines enhancing the well-known growth inhibitor effect of the free EGCG.

Keywords: PLGA, Epigallocatechin-3-gallate (EGCG), Molecular Dynamics (MD) simulation, Drug Delivery System, Poloxamer-407

1- Introduction

Biodegradable polymers are widely used in many different biomedical applications because of their biocompatibility, non-toxic, and non-immunogenic characters, correlated to a minimization of potential adverse local biological responses in the fields of tissue engineering and drug delivery [1]. In this context, the biodegradable medical device can be easily disposed from the body via dissolution, assimilation and excretion through natural metabolic pathways (i.e. citric acid cycle or by direct renal excretion) [2]. Among a wide variety of synthetic biodegradable polymers, the copolymer poly-(lactic-co-glycolic acid) (PLGA) (**Figure 1A**) is the most popular available Food Drug Administration (FDA) approved biodegradable polymer thanks to its long clinical history, good degradation characteristics, and its ability to gradually release small molecules [3,4]. Many publications in the last decade have remarked the potential use of PLGA as efficient drug delivery carrier [5,6]. Moreover, an important part of research involving PLGA polymers has focused from nano-particulate delivery systems characterized by size range between 20 and 100 nm [7–9]. In fact, nanoparticles (NPs) have peculiar physical-chemical properties due to their much smaller size and greater surface area with respect to the corresponding micro-particulate composites, hence offering several advantages. To confirm that, PLGA NPs have been found to protect DNA from degradation in endolysosomes, and are also widely used to deliver hydrophilic/hydrophobic drugs [10], proteins [11] and DNA plasmid [12].

Epigallocatechin 3-Gallate (EGCG) (**Figure 1B**) is the major catechin constituent in green tea [13] with well-known anticancer activity [14–16]. EGCG is also one of the most prominent polyphenols studied for its strong antioxidant properties [17,18], since many different mechanisms contribute to this biological activity [19–23]. However, EGCG beneficial effects are counterposed to poor membrane permeability and chemical instability in physiological environment [24,25]. Although

several drug delivery systems are used at this purpose including lipid-, protein- and polymer-NPs [26–28], the effect of EGCG encapsulation inside the PLGA-based NPs has not been fully explored yet.

In this work, the impact of EGCG concentration on PLGA NPs properties has been studied underlining the importance of the use of an appropriate stabilizer for obtaining colloidal stable NPs. The NPs formulations have been prepared both in the presence of only polyvinyl alcohol (PVA) (**Figure 1C**), a widely used steric stabilizer [29] or using a mixture of PVA and Poloxamer-407 (P407), namely P-F and PP-F respectively. The P407 is an ABA-type triblock copolymer with a centre block of hydrophobic polypropylene oxide (PPO) in between two hydrophilic polyethylene oxide (PEO) lateral chains (**Figure 1D**), characterized by low toxicity and compatibility with the high ability to avoid aggregation among NPs [30,31].

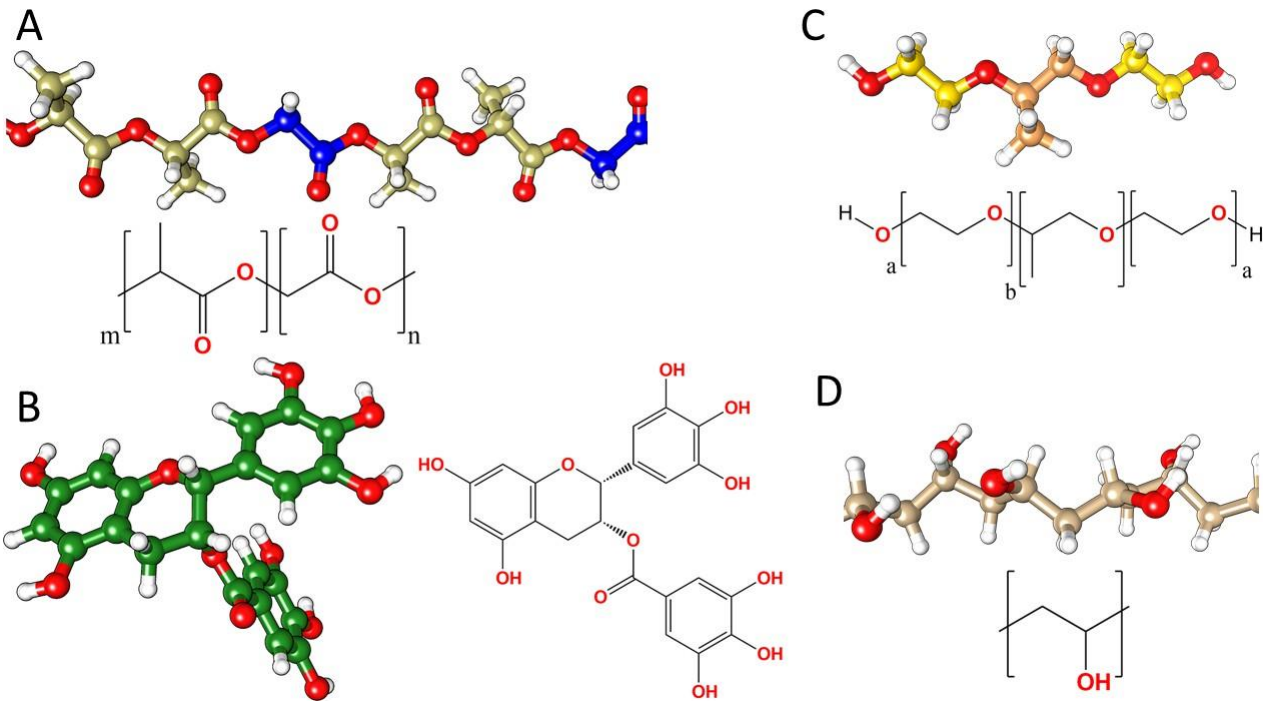

Figure 1: 3D and 2D structures of PLGA (a), EGCG (b), P407 (c), and PVA(d). Oxygen and hydrogen atoms are always reported in red and white respectively, while Carbon atoms colour change in relation to the chemical structure; blue (PGA), tan (PLA), green (EGCG), orange (PPO), yellow (PEO), and brown (PVA).

Despite the great potential of NP-based drug carriers, the lack of specific regulatory guidelines for the characterization of those materials (especially at the early development stage) hinders their clinical potential and commercialization [32,33] [34]. In this perspective, with the aim to operate a complete monitoring of these NPs, a complex study based on different approaches has been carried out. Full-atoms Molecular Dynamics (MD) simulations have been carried out to describe the movements and the interactions of the PLGA-EGCG systems, but also a clear description of the NPs production has been reported with a section concerning the systems characterization. Drug loading, particle size, colloidal stability and morphology studies have been carried out as well. To clarify the molecular interactions between PLGA and EGCG, Attenuated Total Reflectance–Fourier Transform Infrared (ATR-FTIR) spectroscopy has been also used [35]. Finally, the potential toxicity characters of PLGA-EGCG NPs have been tested on non-small cell lung cancer (NSCLC) (A549). The proposed approach, based on combining experimental techniques together with computational methods, provides additional insights into the behaviour of both the polymer NPs alone and EGCG-polymer systems as method to increase the anticancer effect of this polyphenol avoiding harmful and unwanted processes.

2- Materials and Methods

2.1 Computational methods

A polymer system containing 7500 Lactic Acid (LA) units in racemic forms and 2500 Glycolic Acid (GA) units has been prepared to generate 75/25 (LA/GA) PLGA copolymer. To simulate the effects due to polydispersity, each polymer structure has been repeated three times through space with different chain lengths. The resulting PLGA contained 7500 + 7400 + 7300 LA and 2500 + 2467 + 2433 GA units. The random composition of PLGA with 75% PLA and 25% PGA has been chosen to generate polymeric systems at nanoscale level, in accordance with the experimental approaches used in this study. The accuracy in the reproduction of specific size system was due to the need to model

the systems according to their experimental preparation [36]. Each system has been placed in a 52 nm^3 simulation box and solvated with 896,452 three-site transferrable intermolecular potential (TIP3P) water molecules [37]. The three-dimensional structures of EGCG (logP = 1.2; Molecular weight: 458.372 g/mol) molecule has been generated and minimized using semiempirical AM1-BCC method [38]; then, four PLGA have been prepared: free-PLGA, PLGA-1.4 mM EGCG, PLGA-4.3 mM EGCG, PLGA-6.6 mM EGCG. With the aim to reproduce the experimental concentrations, 23, 70, and 107 EGCG molecules have been randomly included inside the three PLGA systems to reach concentrations of 1.4, 4.3, and 6.6 mM respectively. All MD simulations have been performed using GROMACS 5.0.4 suite [39] and CHARMM36 force field [40] with specific parameter extensions to provide an accurate description of EGCG molecules, polymer chains, and to appropriately predict the effect of the solvent. Systems have been minimized applying periodic box conditions (PBC) in all directions, using a neighbour searching grid type; the cut-off distance for the short-range neighbour list was set to 1.4 nm. Electrostatic interactions have been included by implementing a fast smooth particle-mesh Ewald algorithm [41,42] with 1.4 nm distance for the Coulomb cut-off, which is considered the method of choice to obtain an accurate evaluation of long-range electrostatic interactions in large macromolecular systems [43,44].

Each system has been subjected to two minimization steps using steepest descent and conjugate gradient algorithms [45] and subsequent six preliminary equilibration steps based on 5 ns of annealing simulations to gradually reach the simulation temperature of 310 K and generate atomistic velocities. A weak temperature coupling (Berendsen thermostat), with a time constant of 1 ps has been applied to maintain the reference temperature (310 K) throughout the whole run. The subsequent production step consisted in 200 ns of MD simulation in isothermal-isobaric (NPT) ensemble at 1 atm and 310 K. The analysis of the MD trajectories has been performed by means of VMD [46], CHIMERA software [47], and using tools included in the Gromacs package.

2.2. Formulations of EGCG loaded PLGA-NPs

PLGA NPs loaded with EGCG have been prepared using a modified double emulsion/solvent evaporation technique [48]. Briefly, a 0.5 mL aqueous solution containing increasing amount of EGCG has been added to 3 mL PLGA (30 mg) solution in acetone and emulsified using a probe sonicator (QSonica Q125) at 30% amplitude for 30 s. The resulting oil-in-water primary emulsion has been then stirred for 30 min at room temperature and added dropwise (over a period of 3 min) to 3 mL of aqueous solution containing PVA (1% w/v) or mixtures of stabilizers composed of PVA (0.5% w/v) and P407 (0.5% w/v). The obtained double emulsion has been magnetically stirred for 24 h with a subsequent solvent evaporation step using a rotary evaporator for 2 h at 40 °C. Following nanoparticle preparation, suspensions have been washed in distilled water two times at 25.000×g for 15 min at 4°C. The final EGCG concentration in PLGA-NPs was 1.5, 4.5 and 6.5 mM namely P-F1, P-F2 and P-F3 in presence of PVA and PP-F1, PP-F2 and PP-F3 in the case of PVA/P407 addition, respectively. For empty nanoparticle (blank) preparation the same protocol has been used in the absence of EGCG.

2.3. Nanoparticles characterization

2.3.1. Encapsulation efficiency (%) and Drug Loading (%) of EGCG in PLGA-NPs

The EGCG-loaded PLGA-NPs stabilized with PVA (P-F1, P-F2 and P-F3) or with PVA/P407 (PP-F1, PP-F2 and PP-F3) have been purified from the free EGCG by size exclusion chromatography following a well-established procedure [27]. The encapsulation efficiency (EE) and drug loading (LC) of EGCG inside all formulations have been determined by measurement of EGCG concentration in purified and impurified nanoparticles and calculated using the following relationships:

EE (%) = 100 x [amount of EGCG inside nanoparticles/initial amount of EGCG added]

DL (%) = 100 x [amount of EGCG inside nanoparticles/total weight of nanoparticles]

All the experiments have been repeated at least three times and measurements have been run in triplicate.

2.3.2. Dynamic Light Scattering

The intensity-based diameter (Z-average) and the polydispersity index (PDI) of PLGA NPs formulations have been measured by Dynamic Light Scattering (DLS) and Electrophoretic Light Scattering using a Malvern Zetasizer Nano ZS (Malvern Instruments GmbH, Marie-Curie-Straße 4/1, 71083 Herrenberg, Germany). Measurements have been performed at 25 °C with a fixed angle of 173°. The experiments have been performed in PBS and in presence of Fetal Bovine Serum (FBS, 50% v/v). The reported data represent the average of at least three different autocorrelations that have been carried out for each investigated sample

2.3.4. Scanning Electron Microscopy

Scanning electron microscopy (SEM) observations have been performed by a Zeiss Supra 40 field emission electron microscope operating at 5 kV by using the secondary electron signal from the "in lens" detector. Sample preparation consisted in dispersing a single droplet of solution on a polycarbonate filter followed by vacuum drying. Gold coating by sputtering have been carried out after drying to avoid charging effects during SEM observations. Samples have been observed immediately after preparation.

2.3.5. In vitro EGCG release assay

The in vitro EGCG release from PP-F nanoparticles has been studied by the dialysis method after separation of unloaded EGCG by gel-filtration chromatography. Dialysis bags have been soaked in PBS before the use and then rinsed in the same medium. Then, 4 mL of PP-F1, PP-F2, and PP-F3 formulations have been placed in the dialysis bag (12,000 MW cut off) and dialyzed against 30 mL of PBS (pH 7.4). As control, bag containing EGCG alone has been prepared and dialyzed at the same conditions. The dialysis process has been performed under magnetic stirring at 37 °C protecting the

solutions from bright light. At scheduled intervals, 1 mL of the release medium has been collected for the analysis followed by the addition of the same volume of fresh PBS to maintain a constant release volume. The cumulative percentage of EGCG released has been determined from the absorbance measured at 280 nm by a UV–visible spectrophotometer. The calibration curve has been plotted using EGCG in PBS. The percentage released at each time point has been expressed as a fraction of the total amount of EGCG. Drug release has been monitored for 24 h. The data represent the average of three experiments.

2.3.5. ATR-FTIR Measurements

IR spectra have been acquired in reflectance mode using a Perkin Elmer Spectrum GX1 spectrometer, using the ATR accessory equipped with a ZnSe crystal. The spectral range was 4000–550 cm^{-1}, with a spectral resolution of 4 cm^{-1}; each spectrum was the result of 32 scans. Samples have been directly deposited onto the ZnSe crystal without requiring any preparation. Then, five IR spectra have been acquired on each sample. The average absorbance spectrum and the corresponding standard deviation spectra (average absorbance spectrum ± standard deviation spectra) have been calculated before each sample acquisition, the background spectrum being collected on the clean crystal under the same conditions. Raw IR spectra have been converted in absorbance mode and vector normalized (Spectrum 10.4.0 software, Perkin-Elmer). These spectra have been curve-fitted in the 1800−1400 cm^{-1} spectral range; the number and the position of the underlying bands have also been identified by second derivative minima analysis and fixed during the peak-fitting procedure with Gaussian functions; the integrated areas of all the underlying bands have been obtained (GRAMS/AI 9.1, Galactic Industries, Inc., Salem, New Hampshire).

2.4. Cytotoxicity assay on lung cancer cells

The human lung adenocarcinoma epithelial cell line (A549) has been routinely maintained in 25 cm^2 flasks in complete DMEM medium at 37 °C, 5% CO_2, and 95% relative humidity. Complete DMEM medium has been prepared by adding 10% (v/v) FBS, 2 mM glutamine, and 100 U/mL penicillin–

streptomycin. Cells have been detached by trypsinization with trypsin/EDTA solution and counted using trypan blue exclusion assay.

A549 and HDF cells have been seeded in 96-well plates at $5x10^3$/well and $10x10^3$/well, respectively to reach 60% of confluence after 24 h; then, the medium has been removed and replaced with 0.2 mL of fresh culture medium supplemented with increasing amount of PP-F1 and PP-F2 formulation (PLGA, 20, 40, 80, 160, 320 and 640 µg/ml) and incubated for 72 h. Free EGCG has been used as control and it has been added at concentrations equal to the EGCG content tested in the PP-F2 (EGCG, 20, 40 and 80 µM). Cell viability has been assessed by 3-(4,5-dimethylthiazol-2-yl)-2,5-diphenyltetrazolium bromide (MTT) assay following a well-established procedure [49]. After 4 h of MTT incubation, 100 µL of DMSO has been added to each well to solubilize the purple formazan crystals formed after MTT cell reduction. The absorbance has been read on a multiwell scanning microplate reader (BioTek Synergy HT MicroPlate Reader Spectrophotometer, BioTek Instruments Inc., Winooski,VT, USA) at 570 nm using the extraction buffer as a blank. The optical density in the control group (untreated cells) has been considered as 100% viability. The relative cell viability (%) has been calculated as (A570 of treated samples/A570 of untreated samples) x 100. Determinations have been carried out in triplicate in each experiment and mean ± SD has been calculated from five independent experiments.

2.5. Statistical analyses

Data have been presented as mean ±S.D. Statistical comparison of differences among groups of data has been carried out using Student's t-test. $P \leq 0.05$ have been considered statistically significant, while $P \leq 0.001$ have been considered highly significant.

3- Results

3.1. PLGA nanoparticles production and characterization: effect of PVA-Poloxamer-407 stabilizer system

The composition of PLGA nanoparticles, prepared with increasing EGCG concentration (1.4, 4.4 and 6.6 mM) is shown in **Table 1**. Blank formulation, prepared in presence of PVA (1% w/v) solution as an emulsifier, showed a particle size of about 200 nm after 24 h of preparation. The presence of a binary PVA-P407 stabilizer system, both used at final 0.5% w/v concentration, resulted in the formation of smaller sized blank NPs (119 ± 2 nm). The mean diameter of particle size in PBS (pH, 7.4) was influenced by the addition of EGCG, showing a similar trend in both type of formulations. At the lowest EGCG concentration, a decrease in particle size of about 15-20 nm has been observed (P-F1, 185 ± 6 nm; PP-F1, 110 ± 1 nm), while further addition of EGCG determined an increase in their mean diameter. In the formulation P-F3, this resulted in the formation of particles larger than 1 μm that tended to precipitate after 24 h while the simultaneous presence of PVA-P407 in PP-F3 avoided aggregation phenomena although a few precipitates, visible to the nicked eye, was again present after 24 h of preparation. Overall, all formulations were almost neutral (0 > Z potential (mV) < -10) (data not shown). The encapsulation efficiency (%EE) in NPs has been determined after 24 h of preparation. As shown in **Table 1**, in NPs containing only PVA as stabilizer, EE% was found to increase from P-F1 (23%) to PF-2 (39%) followed a decrease at higher EGCG concentration (P-F3, 24%). In this type of formulation, the Drug Loading (DL), which is referred to the amount of total entrapped EGCG with respect to the total polymer weight (PLGA and PVA in P-F; PVA/P407 and PLGA in PP-F), increased until a plateau was achieved at 6.6 mM of EGCG concentration (P-F3). In the presence of the binary PVA/P407 stabilizer system, the %EE and %DL increased in a dose-dependent manner and the percentage obtained have been found to be higher than those of formulations containing only PVA. Overall, the presence of Poloxamer-407 resulted in the formation of NPs with optimum entrapment efficiency and particle size, and therefore they have been selected for the following investigations.

Table 1. Composition and properties of investigated PVA-PLGA-NPs (P-F) and PVA/P407-PLGA-NPs (PP-F).

Formulations	EGCG (mM)	EGCG: PLGA ratio	PVA (%, w/v)	P407 (%w/v)	Time	Particle size ± SD (nm)	PDI±SD (nm)	Encapsulation Efficiency (EE%)	EGCG entrapped (mM)	Drug Loading (DL%)
Blank	-	-	1	-	0 h	208 ± 5	0.15 ± 0.04	-	-	-
					24 h	198 ± 6	0.11 ± 0.01			
P-F1	1.4	1:15	1	-	0 h	185 ± 6	0.18 ± 0.01	23 ± 2	0.32 ± 0.02	0.7
					24 h	214 ± 7	0.17 ± 0.04			
P-F2	4.4	1:5	1	-	0 h	550 ± 20	0.3 ± 0.1	39 ± 5	1.7 ± 0.3	3.9
					24 h	620 ± 50	0.26 ± 0.07			
P-F3	6.6	1:3	1	-	0 h	1496 ± 25	-	24 ± 3	1.6 ± 0.2	3.6
					24 h	-	-			
Blank	-	-	0.5	0.5	0 h	119 ± 2	0.11 ± 0.01	-	-	-
					24 h	122 ± 3	0.09 ± 0.03			
PP-F1	1.4	1:15	0.5	0.5	0 h	110 ± 1	0.08 ± 0.03	49 ± 2	0.71 ± 0.03	1.6
					24 h	113 ± 6	0.17 ± 0.04			
PP-F2	4.4	1:5	0.5	0.5	0 h	134 ± 4	0.09 ± 0.01	58 ± 5	2.4 ± 0.3	5.5
					24 h	129 ± 5	0.12 ± 0.04			
PP-F3	6.6	1:3	0.5	0.5	0 h	150 ± 6	0.07 ± 0.02	61 ± 4	4.1 ± 0.2	9.3
					24 h	345 ± 10	0.43 ± 0.03			

3.2. Colloidal Stability of NPs in serum

The physical stability of EGCG-loaded PP-F NPs has been studied after their exposure to plasma proteins contained in serum. As shown in **Figure 2**, the most stable systems were the empty and PP-F2 which retained a constant mean diameter during the time of analyses. Immediately after serum adding, PP-F1 showed instead an increase in particles size of about 40 nm; however, after 4 h the system appears stable with a mean diameter only slightly higher with respect to PBS condition (**Table 1**). Although the PP-F3 showed a mean diameter of about 130 nm at all times analysed, after 4 h of incubation, a massive flocculation has been observed underlining the colloidal instability induced by the higher EGCG concentration.

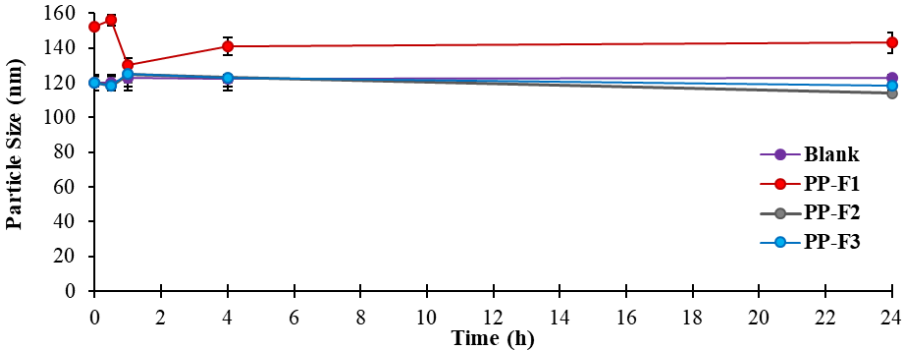

Figure 2. Influence of serum on size distribution of EGCG-based PVA/P407 PLGA NPs.

3.3. Morphological Characterization of EGCG-based PVA/P407 PLGA NPs

The surface morphology of the blank and EGCG-loaded PP-F NPs has been determined by SEM and the results have been shown in **Figure 3**. All NPs appeared to be spherical with a uniform size distribution (**Figure 3C**) except those containing the highest EGCG concentration (**Figure 3D**) that appeared more irregularly shaped. The SEM results confirmed the DLS measurements (**Table 1**), and a progressive increase in mean diameter has been observed.

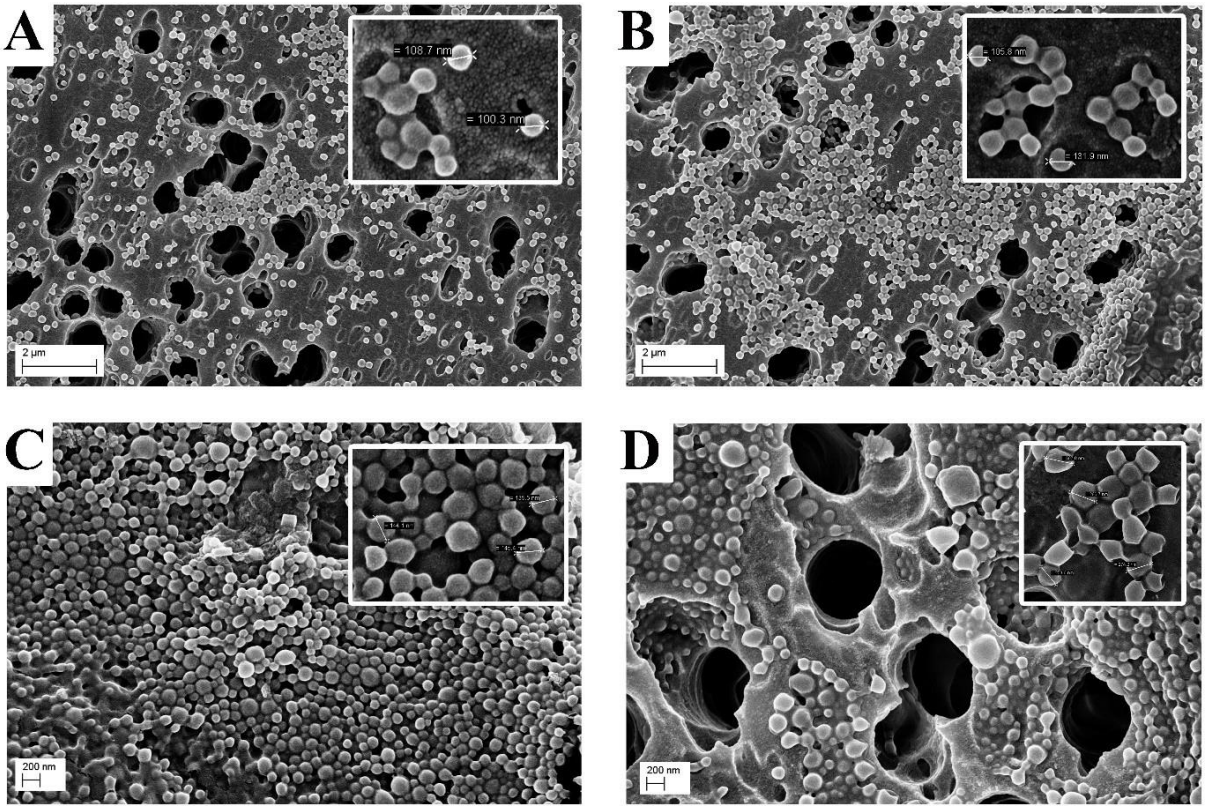

Figure 3. SEM images of PLGA nanoparticles produced in presence of P407 and PVA as stabilizer. (a) Empty PLGA-NPs, (b) PP-F1, (c) PP-F2 and (d), PP-F3 were analysed after preparation (t=0).

3.4. *In vitro* EGCG release profile

The *in vitro* EGCG release profile from PLGA-NPs has been studied by dialysis method at 37 °C in PBS and results expressed as cumulative percentage release during 24 h (**Figure 4**). The release behaviour of free EGCG, used as control, showed a complete diffusion through the dialysis membrane after 6 h confirming our previous results [31]. The EGCG encapsulation inside PVA/P407 PLGA NPs modified its release profile. All formulations showed a similar behaviour in the early phase with an EGCG release after 4 h of 32, 21, and 31% for PP-F1, PP-F2 and PP-F3, respectively. After this time, the EGCG diffusion gradually increased in all NPs. However, the most higher drug release has been observed for the PP-F3 (24 h, 73%). In all cases a complete release of EGCG has never been observed.

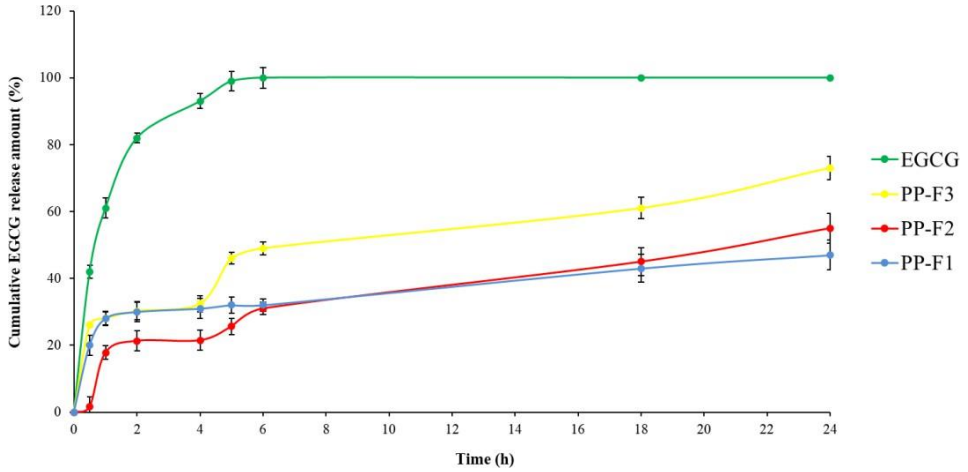

Figure 4. *In vitro* release of EGCG in PBS (pH 7.4) for PP-F1, PP-F2, PP-F3 and free drug solution. Values are expressed as mean ±SD; n = 3 independent experiments.

3.5. ATR-FT-IR Analyses

The interactions between PLGA and EGCG have been studied by ATR spectroscopy, and the relative vibrational spectra have been compared with those of the starting components individually considered. The average infrared spectra of free EGCG (E), Blank, PP-F1, PP-F2, and PP-F3 complexes have been reported in **Figure 5**, where the wavenumbers of the most significant peaks are reported on the top, while have been listed in **Table 2**, together with the corresponding vibrational modes and group assignments.

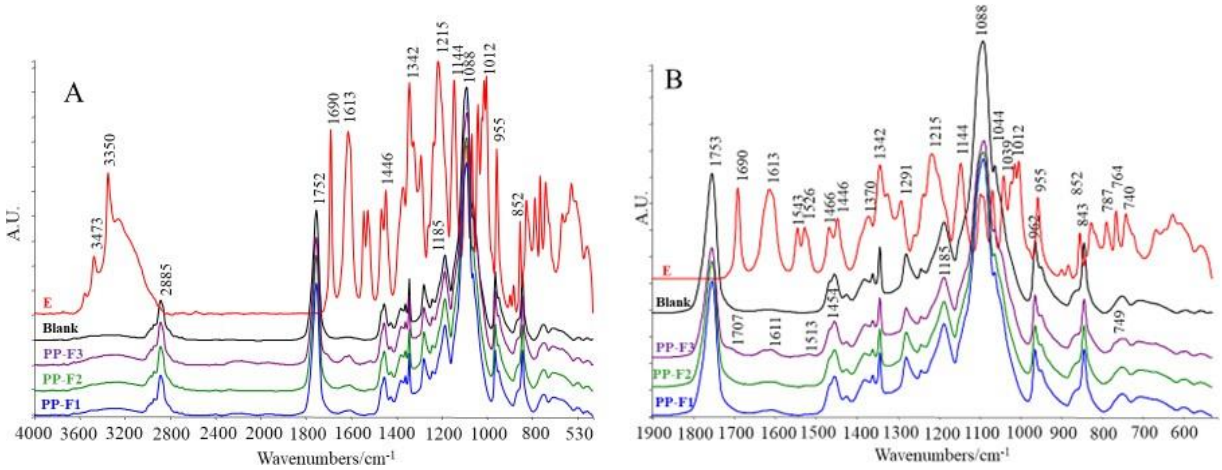

Figure 5: Average absorbance spectra of E, Blank, PP-F1, PP-F2 and PP-F3 samples, in the range 4000-530 cm^{-1} (a) and in the range 1900-500 cm^{-1} (b).

Table 2. Selected IR absorbances of samples E (*), Blank and F1-F3: peak position (in terms of wavenumbers, cm^{-1}), vibrational mode and group assignment. Wavenumbers shown in brackets indicate band shift.

Peak position (cm^{-1})	Molecular assignments
3473*	Stretching modes of free hydroxyl (-OH) group
3350*	Stretching modes of bond hydroxyl (-OH) group
2885	Stretching modes of CH_2 moieties
1753	Stretching mode of carbonyl (C=O) moiety
1690 (1707)*	Stretching mode of carbonyl (C=O) moiety
1613 (1611)*	Stretching mode of -C=C- moiety of the aromatic ring
1543*	Deformation of hydroxyl (-OH) group and stretching of conjugated C-O moieties
1526 (1513)*	Stretching mode of -C=C- moiety of the aromatic ring
1466, 1446*	Bending mode of CH_2 moieties
1453	Bending mode of CH_2 moieties
1370, 1342, 1291*	Deformation of C-H and stretching of C–O moieties
1360, 1342, 1278	Deformation of C-H and stretching of C–O moieties
1215*	Deformation of hydroxyl group
1185	Stretching mode of C-O moiety
1144*	Stretching mode of C-O-C moiety
1088	Stretching of C–O and C-OH moieties
1039 (1044), 1012 (1016)*	Stretching of C–O and C-OH moieties
962, 843	C-H out of plane mode
852*	C-H out of plane bending in phenyl rings
787,764,740*	Stretching of -C=C- aromatic (trisubstitution)
749	Stretching of -C=C- aromatic (trisubstitution)

The infrared spectra obtained exhibited distinct differences, indicating that the complexation induced structurally conformational changes on EGCG. For the polyphenol, the peaks at 3473 and 3350 cm^{-1} are attributed to the stretching of free and associated hydroxyl (-OH) groups respectively, while the peak at 1690 cm^{-1} was due to the carbonyl (C=O). The peaks at 1613 and 1526 cm^{-1} are attributed to the aromatic -C=C- moieties [50]. The three bands at 1370, 1342 and 1291 cm^{-1}, together with those at 1215, 1144, 1039 and 1012 cm^{-1} are typically correlated with C-H, aromatic O-H, C-O-C (C5-O13-C14), alcohol C-OH and C-O moieties respectively [51]. The peaks at 852, 787, 764 and 740 cm^{-1} are attributed to C-H out of plane bending and to the aromatic -C=C- stretching of substituted phenyls. Blank sample showed characteristic peaks at 2885, 1753, 1453, 1360, 1342, 1278, 1185, 1088, 962, 843 and 749 cm^{-1}, and this spectral trend can be observed also in PP-F1, PP-F2 and PP-F3 complexes

(**Figure 5B**), while EGCG characteristic bands have been found only for concentrations equal to or greater than 4.4 mM.

Due to chemical interactions between the polymer matrix and the drug, some characteristic EGCG bands, in particular those at 1690, 1613, 1543, 1039 and 1012 cm^{-1} appeared to be slightly shifted in samples PP-F2 and PP-F3 (**Table 2**). After complexation, the band at 3350 cm^{-1} (hydroxyl group) rapidly decreased and the aromatic O-H nearly vanished.

3.6. Molecular dynamics results

To verify the stability of the EGCG-loaded PLGA-NPs, the dynamic trajectories of polymeric structures have been checked using radius of gyration (R_g) analysis (**Figure 6A**). Starting from the same R_g values for all NPs at the beginning of MD simulations, a univocal behaviour for each system has been detected along MD simulation, since all models showed a gradual decrease of R_g values during the first 100 ns of simulations. Small R_g values indicated that the polymer structure was always relatively compact and adopts a folded structure throughout its trajectory regardless the EGCG amount. Focusing on the last 50 ns of MD simulations, the values reflected dissimilar behaviours in function of the EGCG amount. In fact, the lowest R_g value has been detected for the F1 (3.03 nm), while an increase has been observed in the blank (3.42 nm). Finally, the Rg values increased again moving from F2 (3.69 nm) to F3 systems (4.12 nm). To go deeply inside the behaviour of PLGA-NPs in contact with the simulated environment, the solvent accessible surface area (SASA) has been calculated analysing MD trajectories (**Figure 6B**). SASA plot revealed different behaviours between formulations. In presence of EGCG, the values increased from 800 to 1200 nm^2 in F1 and F2, respectively. Interestingly, the empty PLGA-NPs (blank) showed a SASA value of 1080 nm^2 which is therefore higher with respect the F1 SASA value and lower than those calculated in F2 and F3.

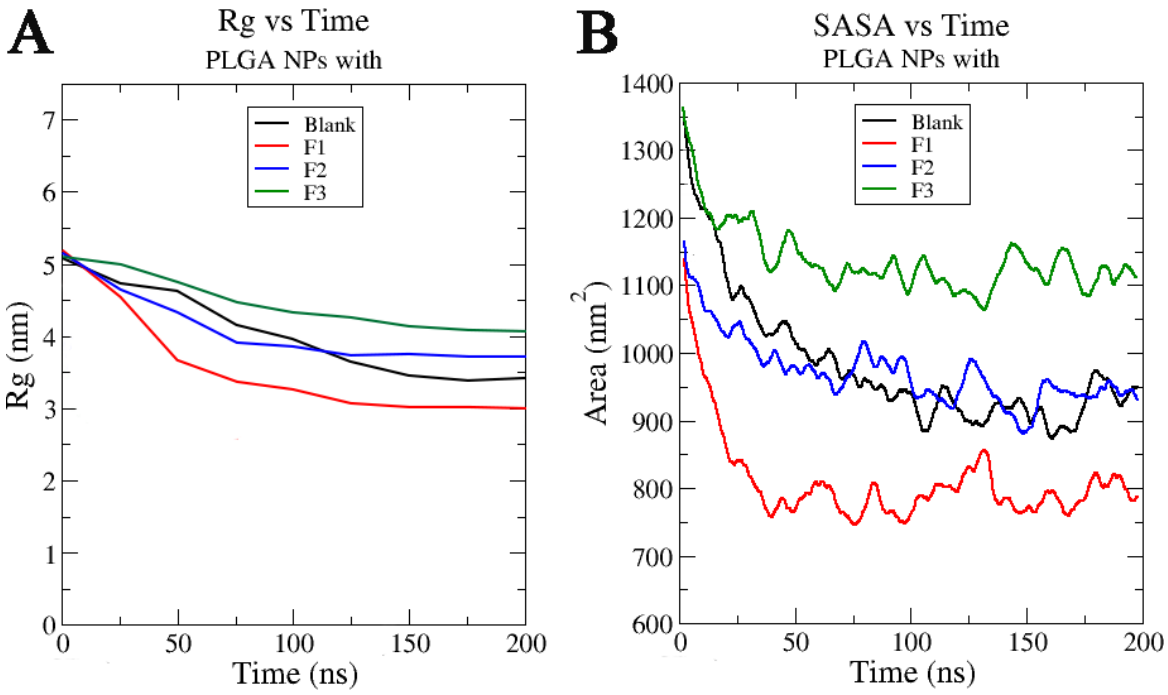

Figure 6. Radius of gyration (a) and solvent accessible surface area (b) of NPs in function of MD simulation time.

Focusing on the individual flexibility of EGCG, in terms of the number of molecules moving and fluctuating during a simulation, root-mean square fluctuation (RMSF) has been calculated following the last 50 ns of MD simulations. Since a different number of molecules were present comparing F1, F2, and F3, an average value comprising all molecules has been reported for each system, and the differences have been underlined in **Figure 7A-B**. RMSF values showed a similar trend for each formulation. By comparison, a decrease in fluctuations has been detected for the aromatic CH groups (atoms 6-12, 2-10, 21-29, 25-33, 39-47, and 43-51) in a EGCG dose-dependent way. In fact, higher concentration of EGCG moiety was associated to a more evident RMSF decrease of such groups. Another interesting RMSF decrease has been observed for the ester group between the gallate moiety (atoms 35, 36, and 37) and the rest of molecule.

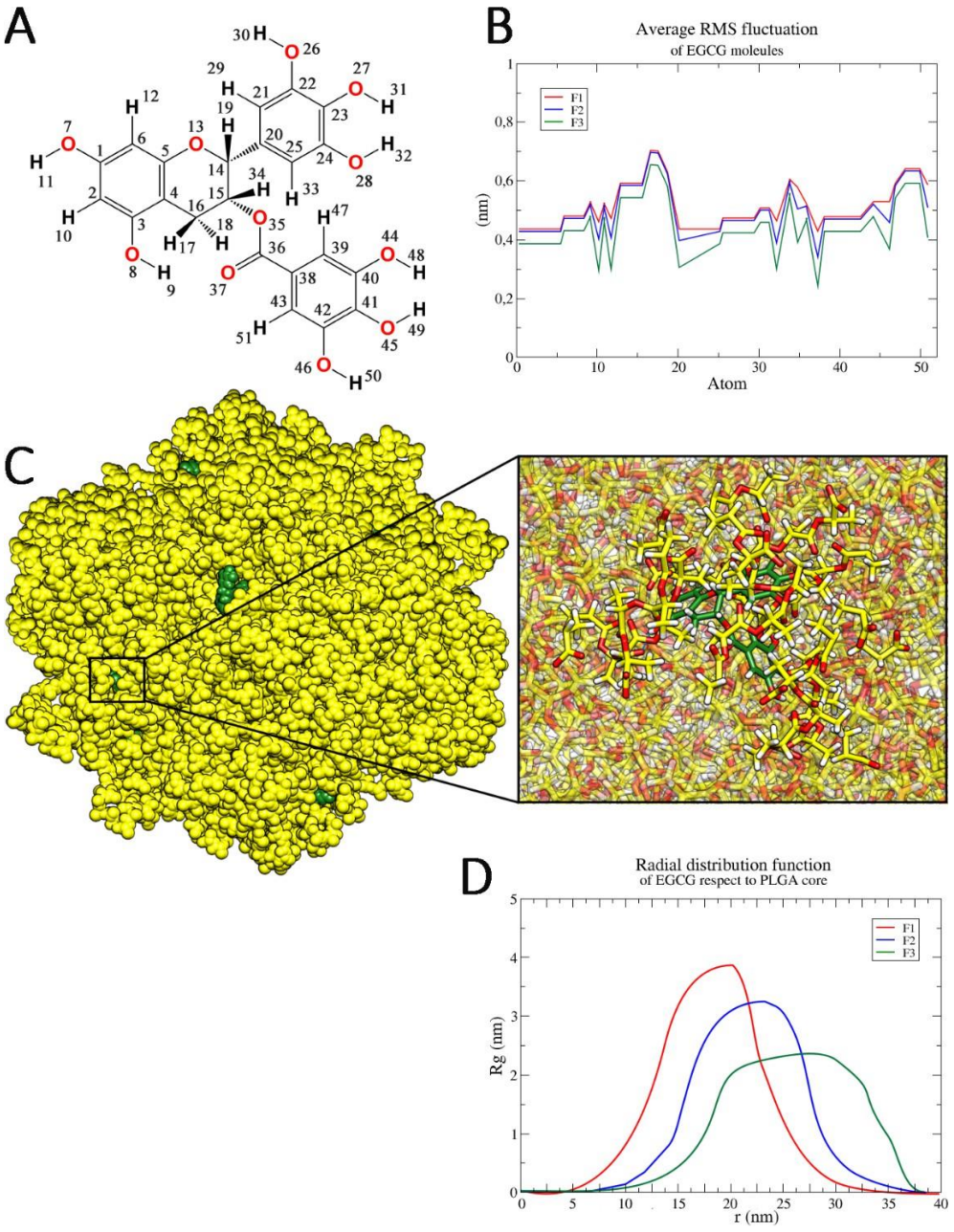

Figure 7. 2D structure (a) and Root-mean-square fluctuation (RMSF) (b) of EGCG molecules. Representative snapshot of PP-F3 at the end of MD simulation. PLGA is reported in yellow, while EGCG is reported in green. In the focus, H and O atoms are reported in white and red respectively (c). Radial distribution function (RDF) of EGCG molecules respect to the PLGA's core (d).

The positions of the EGCG molecules, allowed to freely move within the polymer, have been monitored along MD simulations. As shown in **Figure 7C**, no aggregations have been detected and EGCG moved and diffused inside the PLGA matrix, establishing interactions with polymer. To better

determine the movements of EGCG in polymer formulations, the radial distribution function (RDF) of polyphenol molecules has been calculated (**Figure 7D**). While the molecules in PP-F1 were free to distribute themselves remaining in the PLGA centre, as the concentration increases the EGCG interactions with PLGA NPs surface increased leading to decreased RDF values.

3.7. Cytotoxic effect of EGCG-loaded PLGA in lung cancer cells

The potential anti-cancer application of EGCG-loaded PLGA NPs (PP-Fs) has been assessed in human lung carcinoma A549 cell lines by measuring the percentage of viable cells via MTT assay and comparing with free EGCG (**Figure 8**). Since the PP-F3 showed the presence of precipitates after 24 h of preparation both in PBS and in presence of plasma proteins, only the colloidal stable formulations (PP-F1 and PP-F2) have been selected for this experiment. However, since PP-F2 showed about a double concentration of EGCG entrapped at the same amount of polyphenol tested, the concentration of PLGA administered was different (**Figure 8A-B**). Blank NPs did not affect the viability of A549 cells in the range of PLGA 0-320 µg/ml; above this concentration a cytotoxic effect has been observed with a decrease in cell viability of about 45% (*P<0.001). PP-F1 showed a slight additional cytotoxic effect with respect to blank NPs (**Figure 8A**) while PP-F2 induced a higher decreased in cell viability (**Figure 8B**). As shown in the **Figure 8C**, after a 72 h treatment, free EGCG induced a dose-dependent cytotoxicity in lung cancer cell with a decrease in cell viability of about 40% at 80 µM, thus confirming our previous results [16]. Therefore, to compare the PP-F2 cytotoxicity with that of free EGCG, polyphenol concentrations of 20, 40 and 80 µM have been selected, corresponding to PLGA 80, 160 and 320 µg/ml, respectively (**Figure 8C**). At these doses, PLGA did not induce a significative cell growth inhibition while the PP-F2 potentiated the cytotoxic effect of free EGCG. In particular, the best result has been obtained at 40 µM of EGCG concentration in which a decrease in cell viability of 25% and 45% has been observed with respect to free EGCG and blank NPs, respectively (*P<0.001).

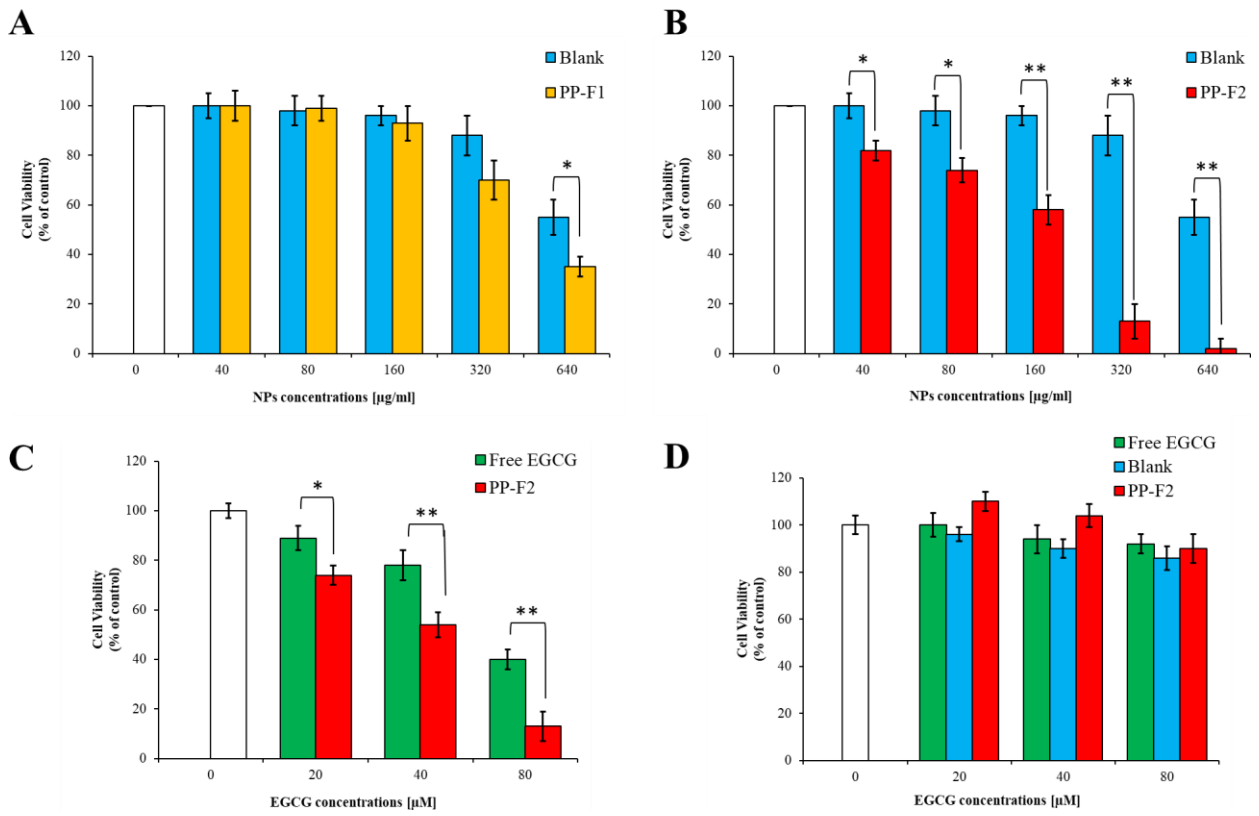

Figure 8. Cytotoxicity of EGCG-loaded PLGA in A549 and HDF cell lines. A549 cells have been treated with increasing concentrations of blank NPs and PP-F1 or PP-F2 at PLGA concentrations range of 0–640 µg/mL for 72 h (a, b) A549 cells were treated with increasing EGCG concentrations (20, 40 and 80 µM) corresponding to PLGA 80, 160 and 320 µg/mL for the PP-F2. Cell viability was measured after 72 h of treatment by MTT assay (c). HDF cells were treated with increasing EGCG concentrations (20, 40 and 80 µM), blank NPs and PP-F2 (PLGA 80, 160 and 320 µg/mL) (d). Data are expressed as means ± S.D. of five independent experiments, each performed in triplicate. *P ≤ 0.05 and **P ≤ 0.001.

To determine if the cytotoxic effect was selective for the cancer cells, the Human Dermal Fibroblasts (HDF) have been used as normal and healthy cell model. At concentrations tested, the EGCG showed a low cytotoxicity on fibroblasts confirming the literature data [52,53] (**Figure 8D**). As for the A549 cells, the blank NPs showed no cytotoxic effect on HDF; therefore, it not surprising that the EGCG-loaded NPs did not affect fibroblasts viability.

4- Discussion

PLGA is one of the most interesting and promising polymers among those commonly used in the biological and biomedical fields, whose different stabilizing effects allow to modify drug-loading capacities, particle size, and colloidal stability in the PLGA nanoparticles [54]; they also represent one of the most important components of polymeric nanoparticles. At the same time, drugs encapsulation inside nanoparticles could influence their physical-chemical properties. In this work, different PLGA formulations stabilized with PVA (1% w/v) have been investigated as delivery systems of EGCG by changing the amount of polyphenol loaded. We confirmed that at the lowest PLGA:EGCG ratio (1:15, **Table 1**), the system was a stable colloid, as reported for the PLGA-PVA NPs loaded with EGCG and prepared in the similar condition. As we previously reported [27,31], higher EGCG concentration strongly affects the particles size and the colloidal stability of nanoparticles resulting in the aggregation/precipitation, which could be related to the formation of several hydrogen bonds (HB) between EGCG and PLGA. Interestingly, the addition of P407, delayed the precipitation phenomena and improved the encapsulation efficiency of EGCG inside PVA/P407 NPs (PP-F). The presence of this stabilizer seems to influence the interaction between PLGA and EGCG, probably by promoting additional interactions with the hydrophilic portions of the P407 (**Figure 9**). However, at higher PLGA:EGCG ratio (1:3, **Table 1**), the presence of a few precipitates underlines the well-known aggregation effect induced by higher EGCG concentrations on nanoparticles. Overall, independently of the stabilizer type used, the effect of EGCG in particle size of formulations (F) follows a similar trend in the P-F and PP-F NPs.

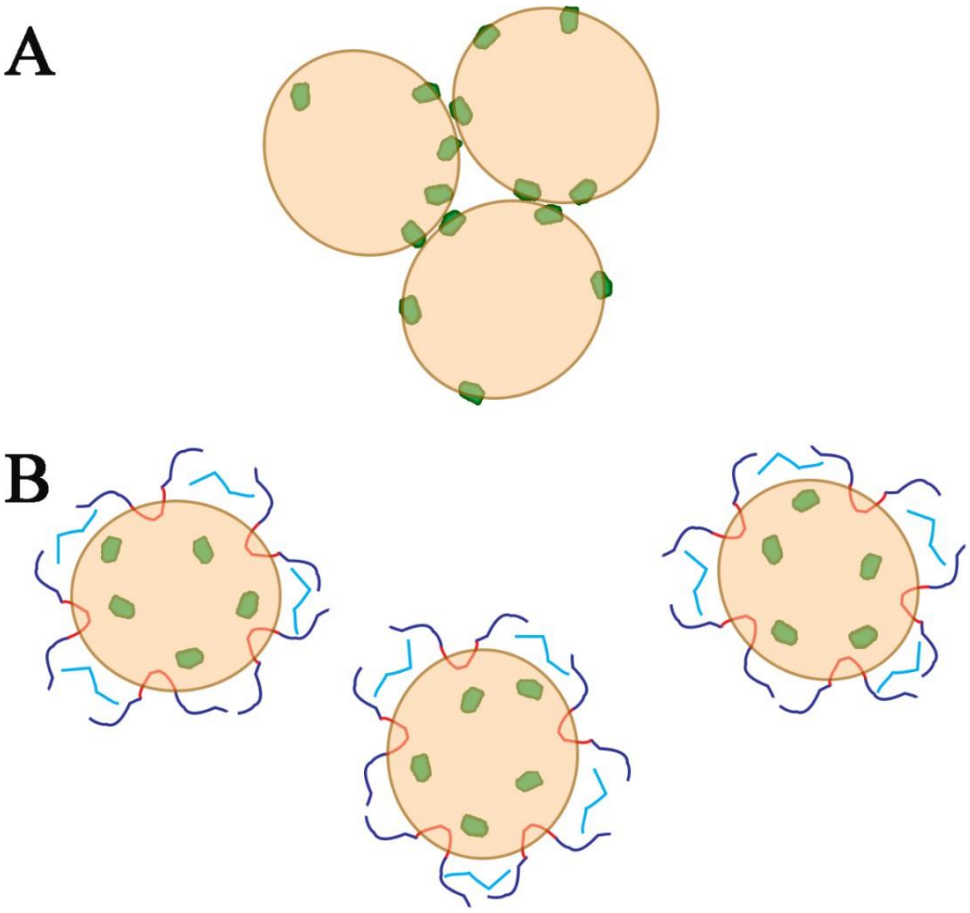

Figure 9. NPs stability without (a) and with PVA/P407 (b). PLGA systems are reported in orange, while EGCG molecules are represented in green. In the figure B, red and blue lines are the hydrophilic PPO and the hydrophobic PEO segments respectively, while the lines in light blue indicate the PVA polymers.

MD simulation has been then used to describe in detail the role of EGCG concentration on physiochemical features of PLGA NPs. Since full-atoms calculations have been performed, the explicit inclusion of PVA and P-407 molecules in simulation boxes resulted difficult to achieve, due to an important increase in the computational efforts. For this reason, and with the aim to avoid possible simulation artifacts, PP-F NPs have not been modelled, while only F NPs have been considered with *in silico* methods. The calculated Rg confirmed the trend observed in the measurements of hydrodynamic diameter size of NPs (**Figure 10**). Therefore, from the results obtained, a lower amount of EGCG led to more compact and folded NPs with respect to the blank and to the other formulations (F2 and F3). The above reported PLGA-EGCG behavior has been

further confirmed by SASA analyses, which revealed a direct correlation with the amount of EGCG loaded. The F1 displayed the lowest SASA value which indicated a very low miscibility degree with the water phase. Therefore, we can assume that, in this condition, the EGCG molecules increased the attractive interactions between PLGA chains acting as a bridge and resulting in an overall lower affinity to the solvent compared to the other two formulations. Interestingly, the calculated RDF showed that in the F1, EGCG molecules were retained in the PLGA center confirming this hypothesis. As the concentration of EGCG increases, a higher mean diameter, SASA and Rg values have been observed. In this case, there was a greater tendency of EGCG to interact with the PLGA surface and water molecules, increasing the hydration shell of NPs. In fact, the decrease in RDF value demonstrated that EGCG was localized mainly at the interface PLGA-water (**Figure 7D**). This EGCG surficial localization is accentuated in the F3 formulation; probably, this could explain the higher tendency of PP-F3 to release EGCG as observed in the *in vitro* release studies (**Figure 4**).

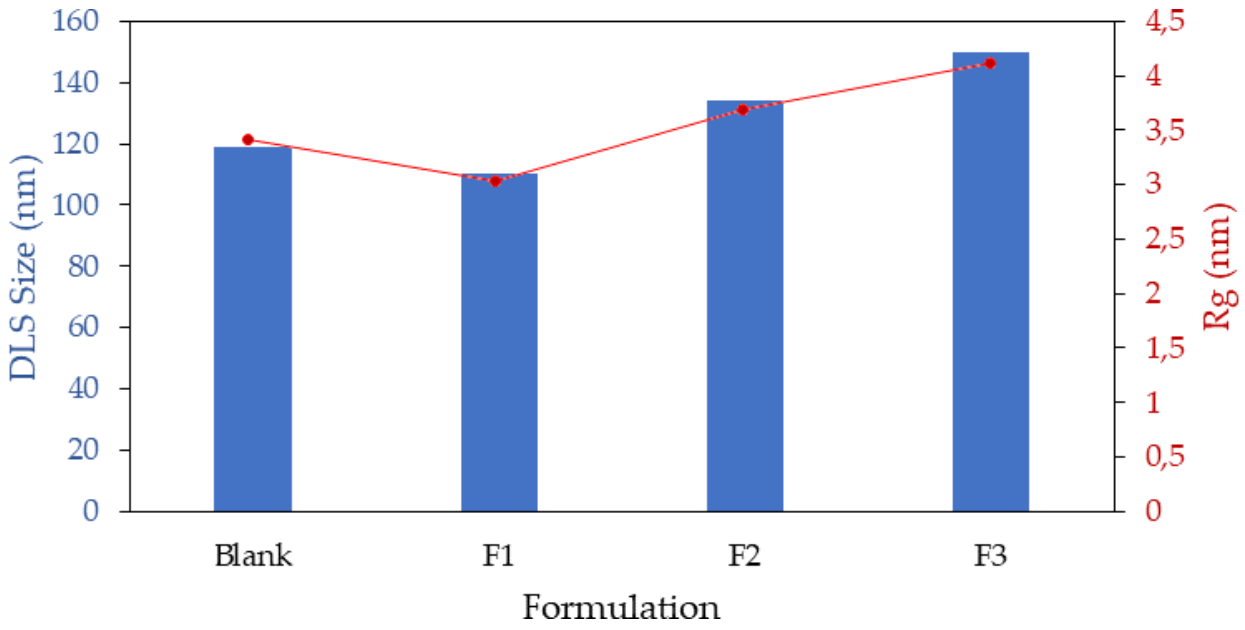

Figure 10. Correlation between NPs size (from DLS) and Rg (from MD).

It is important to underline that EGCG, as well as other natural molecules, tended to clusterize avoiding a correct administration in drug delivery methodologies [55]. However, in this case no

aggregation phenomena have been found between the EGCG molecules. The RMSF data revealed that the main groups involved in the PLGA:EGCG interaction is the ester moiety and the aromatic CH groups of polyphenol molecules. Also in this case a good agreement with IR spectra has been found, since the corresponding peaks showed that a little amount of EGCG may be present on the nanoparticles surface, especially in PP-F2 and PP-F3. The peaks analysis clearly confirmed that EGCG was mainly encapsulated in the core of PLGA-NPs, although a little amount of EGCG could be likely present on the nanoparticles surface. Finally, the spectral trend confirmed that EGCG was quite only present inside the core of NPs, even if in samples PP-F3 it could interact with the surface through the OH groups.

The PP-F2, which is one of the produced NPs, potentiated the cytotoxicity effect of EGCG (25%-fold decrease with respect to the free EGCG) (**Figure 8**) in non-small cell lung cancer (NSCLC) cell line A549 underlining the potential application of EGCG-loaded PVA/P407-PLGA NPs as anticancer delivery system. Moreover, the cytotoxicity studies performed on non-cancer cell model (HDF cell line) indicated that PP-F2 did not affect the cell viability at the concentration tested. In fact, EGCG represent one of main antioxidants molecules in green tea. It exerts several health-promoting effects such as antioxidant and anticancer activities. Multiple mechanisms contribute to the overall antioxidant activity (radical scavenging activity, chelation of transition metals, and ability to increase the expression of antioxidant enzymes). In this context, it has been demonstrated that EGCG in normal cells, such as fibroblasts, shows a low cytotoxicity and protect cells from oxidative stress induced cell death [53,56,57]. The EGCG cytotoxicity in cancer cells has been ascribed to its ability to interact with a wide range of biological targets such as EGFR [16], and NF-κB signaling [58]. Therefore, we can conclude that EGCG has a cancer-selective effect on A549 cells with respect to HDF as just described in other cytotoxicity comparison between normal and cancer cells [59].

5- Conclusions

In this study the possible use of PLGA as delivery system for EGCG has been investigated. Results showed that the anti-aggregating role of P407 on PLGA NPs and that the addition of EGCG strongly influence the mean diameter of the systems. The present study confirmed that PLGA-EGCG NPs give raise to stable systems and allow to deliver the loaded polyphenols. Moreover, this formulation resulted effective against the NSCLC. The adopted methodology, based on combining *in silico* with *in vitro* approaches, indicates that by using this formulation strategy this green tea polyphenol could be delivered in physiologically active concentrations. Finally, the outcome of this study could have direct practical implication, with translational relevance in human lung cancer patients.

Acknowledgements

We would like to thank CINECA-HPC ISCRA MARCONI-100 computer system (NANO-PR project n. HP10CK3EZ0) for the calculations on GROMACS.

References

1. Tian, H.; Tang, Z.; Zhuang, X.; Chen, X.; Jing, X. Biodegradable synthetic polymers: Preparation, functionalization and biomedical application. *Prog. Polym. Sci.* 2012.
2. da Silva, D.; Kaduri, M.; Poley, M.; Adir, O.; Krinsky, N.; Shainsky-Roitman, J.; Schroeder, A. Biocompatibility, biodegradation and excretion of polylactic acid (PLA) in medical implants and theranostic systems. *Chem. Eng. J.* **2018**, doi:10.1016/j.cej.2018.01.010.
3. Lee, J.H.; Yeo, Y. Controlled drug release from pharmaceutical nanocarriers. *Chem. Eng. Sci.* **2015**, *125*, 75–84, doi:10.1016/j.ces.2014.08.046.
4. Ramot, Y.; Haim-Zada, M.; Domb, A.J.; Nyska, A. Biocompatibility and safety of PLA and its copolymers. *Adv. Drug Deliv. Rev.* 2016, *107*, 153–162.

5. Mir, M.; Ahmed, N.; Rehman, A. ur Recent applications of PLGA based nanostructures in drug delivery. *Colloids Surfaces B Biointerfaces* 2017.

6. Perinelli, D.R.; Cespi, M.; Bonacucina, G.; Palmieri, G.F. PEGylated polylactide (PLA) and poly (lactic-co-glycolic acid) (PLGA) copolymers for the design of drug delivery systems. *J. Pharm. Investig.* 2019.

7. Colzani, B.; Biagiotti, M.; Speranza, G.; Dorati, R.; Modena, T.; Conti, B.; Tomasi, C.; Genta, I. Smart Biodegradable Nanoparticulate Materials: Poly-lactide-co-glycolide Functionalization with Selected Peptides. *Curr. Nanosci.* **2015**, doi:10.2174/1573413712666151116213330.

8. Elmowafy, E.M.; Tiboni, M.; Soliman, M.E. Biocompatibility, biodegradation and biomedical applications of poly(lactic acid)/poly(lactic-co-glycolic acid) micro and nanoparticles. *J. Pharm. Investig.* 2019.

9. Casalini, T.; Rossi, F.; Castrovinci, A.; Perale, G. A Perspective on Polylactic Acid-Based Polymers Use for Nanoparticles Synthesis and Applications. *Front. Bioeng. Biotechnol.* 2019.

10. Cohen-Sela, E.; Chorny, M.; Koroukhov, N.; Danenberg, H.D.; Golomb, G. A new double emulsion solvent diffusion technique for encapsulating hydrophilic molecules in PLGA nanoparticles. *J. Control. Release* **2009**, doi:10.1016/j.jconrel.2008.09.073.

11. Feczkó, T.; Tóth, J.; Dósa, G.; Gyenis, J. Optimization of protein encapsulation in PLGA nanoparticles. *Chem. Eng. Process. Process Intensif.* **2011**, doi:10.1016/j.cep.2011.06.008.

12. Jo, A.; Ringel-Scaia, V.M.; McDaniel, D.K.; Thomas, C.A.; Zhang, R.; Riffle, J.S.; Allen, I.C.; Davis, R.M. Fabrication and characterization of PLGA nanoparticles encapsulating large CRISPR-Cas9 plasmid. *J. Nanobiotechnology* **2020**, doi:10.1186/s12951-019-0564-1.

13. Bianchi, A.; Marchetti, N.; Scalia, S. Photodegradation of (-)-epigallocatechin-3-gallate in

topical cream formulations and its photostabilization. *J. Pharm. Biomed. Anal.* **2011**, *56*, 692–697, doi:10.1016/j.jpba.2011.07.007.

14. Zhang, G.; Wang, Y.; Zhang, Y.; Wan, X.; Li, J.; Liu, K.; Wang, F.; Liu, Q.; Yang, C.; Yu, P.; et al. Anti-Cancer Activities of Tea Epigallocatechin-3-Gallate in Breast Cancer Patients under Radiotherapy. *Curr. Mol. Med.* **2012**, *12*, 163–176, doi:10.2174/156652412798889063.

15. Deng, Y.T.; Lin, J.K. EGCG inhibits the invasion of highly invasive CL1-5 lung cancer cells through suppressing MMP-2 expression via JNK signaling and induces G2/M arrest. *J. Agric. Food Chem.* **2011**, *59*, 13318–13327, doi:10.1021/jf204149c.

16. Minnelli, C.; Cianfruglia, L.; Laudadio, E.; Giovanna, M.; Galeazzi, R.; Armeni, T. Effect of epigallocatechin-3-gallate on egfr signaling and migration in non-small cell lung cancer. *Int. J. Mol. Sci.* **2021**, *22*, doi:10.3390/ijms222111833.

17. Lin, F.R.; Niparko, J.K.; Ferrucci, and L. 基因的改变NIH Public Access. *Bone* **2014**, *23*, 1–7, doi:10.1016/j.semcancer.2007.06.013.Inhibition.

18. Minnelli, C.; Galeazzi, R.; Laudadio, E.; Amici, A.; Rusciano, D.; Armeni, T.; Cantarini, M.; Stipa, P.; Mobbili, G. Monoalkylated epigallocatechin-3-gallate (C18-EGCG) as novel lipophilic EGCG derivative: Characterization and antioxidant evaluation. *Antioxidants* **2020**, *9*, doi:10.3390/antiox9030208.

19. Lúcio, M.; Ferreira, H.; Lima, J.L.F.C.; Reis, S. Use of liposomes as membrane models to evaluate the contribution of drug-membrane interactions to antioxidant properties of etodolac. *Redox Rep.* **2008**, *13*, 225–236, doi:10.1179/135100008X308939.

20. Nanjo, F.; Mori, M.; Goto, K.; Hara, Y. Radical scavenging activity of tea catechins and their related compounds. *Biosci. Biotechnol. Biochem.* **1999**, *63*, 1621–1623,

doi:10.1271/bbb.63.1621.

21. Mandel, S.; Amit, T.; Bar-Am, O.; Youdim, M.B.H. Iron dysregulation in Alzheimer's disease: Multimodal brain permeable iron chelating drugs, possessing neuroprotective-neurorescue and amyloid precursor protein-processing regulatory activities as therapeutic agents. *Prog. Neurobiol.* **2007**, *82*, 348–360, doi:10.1016/j.pneurobio.2007.06.001.

22. Simos, Y. V.; Verginadis, I.I.; Toliopoulos, I.K.; Velalopoulou, A.P.; Karagounis, I. V.; Karkabounas, S.C.; Evangelou, A.M. Effects of catechin and epicatechin on superoxide dismutase and glutathione peroxidase activity, in vivo. *Redox Rep.* **2012**, *17*, 181–186, doi:10.1179/1351000212Y.0000000020.

23. Chu, C.; Deng, J.; Man, Y.; Qu, Y. Green Tea Extracts Epigallocatechin-3-gallate for Different Treatments. *Biomed Res. Int.* **2017**, *2017*, doi:10.1155/2017/5615647.

24. Chen, Z.Y.; Zhu, Q.Y.; Tsang, D.; Huang, Y. Degradation of green tea catechins in tea drinks. *J. Agric. Food Chem.* **2001**, *49*, 477–482, doi:10.1021/jf000877h.

25. Lambert, J.D.; Yang, C.S. Cancer chemopreventive activity and bioavailability of tea and tea polyphenols. *Mutat. Res. - Fundam. Mol. Mech. Mutagen.* **2003**, *523–524*, 201–208, doi:10.1016/S0027-5107(02)00336-6.

26. Li, K.; Teng, C.; Min, Q. Advanced Nanovehicles-Enabled Delivery Systems of Epigallocatechin Gallate for Cancer Therapy. *Front. Chem.* **2020**, *8*, 1–9, doi:10.3389/fchem.2020.573297.

27. Minnelli, C.; Moretti, P.; Laudadio, E.; Gerelli, Y.; Pigozzo, A.; Armeni, T.; Galeazzi, R.; Mariani, P.; Mobbili, G. Tuning curvature and phase behavior of monoolein bilayers by epigallocatechin-3-gallate: Structural insight and cytotoxicity. *Colloids Surfaces B Biointerfaces* **2022**, *209*, 112171, doi:10.1016/j.colsurfb.2021.112171.

28. Kazi, J.; Sen, R.; Ganguly, S.; Jha, T.; Ganguly, S.; Chatterjee Debnath, M. Folate decorated

epigallocatechin-3-gallate (EGCG) loaded PLGA nanoparticles; in-vitro and in-vivo targeting efficacy against MDA-MB-231 tumor xenograft. *Int. J. Pharm.* **2020**, *585*, 119449, doi:10.1016/j.ijpharm.2020.119449.

29. Astete, C.E.; Sabliov, C.M. Synthesis and characterization of PLGA nanoparticles. *J. Biomater. Sci. Polym. Ed.* **2006**, *17*, 247–289, doi:10.1163/156856206775997322.

30. Dumortier, G.; Grossiord, J.L.; Agnely, F.; Chaumeil, J.C. A review of poloxamer 407 pharmaceutical and pharmacological characteristics. *Pharm. Res.* **2006**, *23*, 2709–2728, doi:10.1007/s11095-006-9104-4.

31. Minnelli, C.; Moretti, P.; Fulgenzi, G.; Mariani, P.; Laudadio, E.; Armeni, T.; Galeazzi, R.; Mobbili, G. A Poloxamer-407 modified liposome encapsulating epigallocatechin-3-gallate in the presence of magnesium: Characterization and protective effect against oxidative damage. *Int. J. Pharm.* **2018**, doi:10.1016/j.ijpharm.2018.10.004.

32. Miernicki, M.; Hofmann, T.; Eisenberger, I.; von der Kammer, F.; Praetorius, A. Legal and practical challenges in classifying nanomaterials according to regulatory definitions. *Nat. Nanotechnol.* 2019.

33. Sarmento, B. Have nanomedicines progressed as much as we'd hoped for in drug discovery and development? *Expert Opin. Drug Discov.* 2019.

34. Pandey, R.K.; Prajapati, V.K. Molecular and immunological toxic effects of nanoparticles. *Int. J. Biol. Macromol.* 2018.

35. Siano, F.; Moccia, S.; Picariello, G.; Russo, G.L.; Sorrentino, G.; Di Stasio, M.; La Cara, F.; Volpe, M.G. Comparative study of chemical, biochemical characteristic and ATR-FTIR analysis of seeds, oil and flour of the edible Fedora cultivar hemp (Cannabis sativa L.). *Molecules* **2019**, *24*, 1–13, doi:10.3390/molecules24010083.

36. Liechty, W.B.; Kryscio, D.R.; Slaughter, B. V.; Peppas, N.A. Polymers for drug delivery

systems. *Annu. Rev. Chem. Biomol. Eng.* **2010**, doi:10.1146/annurev-chembioeng-073009-100847.

37. Mark, P.; Nilsson, L. Structure and dynamics of the TIP3P, SPC, and SPC/E water models at 298 K. *J. Phys. Chem. A* **2001**, *105*, 9954–9960, doi:10.1021/jp003020w.

38. Jakalian, A.; Jack, D.B.; Bayly, C.I. Fast, efficient generation of high-quality atomic charges. AM1-BCC model: II. Parameterization and validation. *J. Comput. Chem.* **2002**, *23*, 1623–1641, doi:10.1002/jcc.10128.

39. Abraham, M.J.; Murtola, T.; Schulz, R.; Páll, S.; Smith, J.C.; Hess, B.; Lindah, E. Gromacs: High performance molecular simulations through multi-level parallelism from laptops to supercomputers. *SoftwareX* **2015**, *1–2*, 19–25, doi:10.1016/j.softx.2015.06.001.

40. Ashutosh Tripathi, Aaron H. Nile, and V.A.B.; Zhao, H. 乳鼠心肌提取 HHS Public Access. *Physiol. Behav.* **2017**, *176*, 139–148, doi:10.1038/nmeth.4067.CHARMM36m.

41. Darden, T.; York, D.; Pedersen, L. Particle mesh Ewald: An N·log(N) method for Ewald sums in large systems. *J. Chem. Phys.* **1993**, *98*, 10089–10092, doi:10.1063/1.464397.

42. Páll, S.; Hess, B. A flexible algorithm for calculating pair interactions on SIMD architectures. *Comput. Phys. Commun.* **2013**, *184*, 2641–2650, doi:10.1016/j.cpc.2013.06.003.

43. Eastwood, J.W.; Hockney, R.W.; Lawrence, D.N. P3M3DP-The three-dimensional periodic particle-particle/ particle-mesh program. *Comput. Phys. Commun.* **1980**, *19*, 215–261, doi:10.1016/0010-4655(80)90052-1.

44. Stipa, P.; Marano, S.; Galeazzi, R.; Minnelli, C.; Laudadio, E. Molecular dynamics simulations of quinine encapsulation into biodegradable nanoparticles: A possible new strategy against Sars-CoV-2. *Eur. Polym. J.* **2021**, *158*, 110685,

doi:10.1016/j.eurpolymj.2021.110685.

45. Laudadio, E.; Galeazzi, R.; Mobbili, G.; Minnelli, C.; Barbon, A.; Bortolus, M.; Stipa, P. Depth Distribution of Spin-Labeled Liponitroxides within Lipid Bilayers: A Combined EPR and Molecular Dynamics Approach. *ACS Omega* **2019**, *4*, 5029–5037, doi:10.1021/acsomega.8b03395.

46. Zhang, R.; Gao, C.; Pan, S.; Shang, R. Fusion of GNSS and speedometer based on VMD and its application in bridge deformation monitoring. *Sensors (Switzerland)* **2020**, *20*, doi:10.3390/s20030694.

47. Pettersen, E.F.; Goddard, T.D.; Huang, C.C.; Couch, G.S.; Greenblatt, D.M.; Meng, E.C.; Ferrin, T.E. UCSF Chimera - A visualization system for exploratory research and analysis. *J. Comput. Chem.* **2004**, *25*, 1605–1612, doi:10.1002/jcc.20084.

48. Salvador, A.; Sandgren, K.J.; Liang, F.; Thompson, E.A.; Koup, R.A.; Pedraz, J.L.; Hernandez, R.M.; Loré, K.; Igartua, M. Design and evaluation of surface and adjuvant modified PLGA microspheres for uptake by dendritic cells to improve vaccine responses. *Int. J. Pharm.* **2015**, *496*, 371–381, doi:10.1016/j.ijpharm.2015.10.037.

49. Minnelli, C.; Laudadio, E.; Galeazzi, R.; Barucca, G.; Notarstefano, V.; Cantarini, M.; Armeni, T.; Mobbili, G. Encapsulation of a neutral molecule into a cationic clay material: Structural insight and cytotoxicity of resveratrol/layered double hydroxide/BSA nanocomposites. *Nanomaterials* **2020**, doi:10.3390/nano10010033.

50. Zhang, H.; Luo, R.; Li, W.; Wang, J.; Maitz, M.F.; Wang, J.; Wan, G.; Chen, Y.; Sun, H.; Jiang, C.; et al. Epigallocatechin gallate (EGCG) induced chemical conversion coatings for corrosion protection of biomedical MgZnMn alloys. *Corros. Sci.* **2015**, *94*, 305–315, doi:10.1016/j.corsci.2015.02.015.

51. Lee, B.S.; Lee, C.C.; Lin, H.P.; Shih, W.A.; Hsieh, W.L.; Lai, C.H.; Takeuchi, Y.; Chen,

Y.W. A functional chitosan membrane with grafted epigallocatechin-3-gallate and lovastatin enhances periodontal tissue regeneration in dogs. *Carbohydr. Polym.* **2016**, *151*, 790–802, doi:10.1016/j.carbpol.2016.06.026.

52. Li, Q.; Guan, X.; Wu, P.; Wang, X.; Zhou, L.; Tong, Y.; Ren, R.; Leung, K.S.M.; Lau, E.H.Y.; Wong, J.Y.; et al. Early Transmission Dynamics in Wuhan, China, of Novel Coronavirus–Infected Pneumonia. *N. Engl. J. Med.* 2020, *382*, 1199–1207.

53. Han, D.W.; Lee, M.H.; Kim, H.H.; Hyon, S.H.; Park, J.C. Epigallocatechin-3-gallate regulates cell growth, cell cycle and phosphorylated nuclear factor-κB in human dermal fibroblasts. *Acta Pharmacol. Sin.* **2011**, *32*, 637–646, doi:10.1038/aps.2011.17.

54. Agrahari, V.; Mitra, A.K. Therapeutic Delivery. *Ther. Deliv* **2016**, *7*, 117–138.

55. Laudadio, E.; Mobbili, G.; Minnelli, C.; Massaccesi, L.; Galeazzi, R. Salts Influence Cathechins and Flavonoids Encapsulation in Liposomes: A Molecular Dynamics Investigation. *Mol. Inform.* **2017**, *36*, 1–13, doi:10.1002/minf.201700059.

56. Zhang, Q.; Wu, Y.; Guan, Y.; Ling, F.; Li, Y.; Niu, Y. Epigallocatechin gallate prevents senescence by alleviating oxidative stress and inflammation in WI-38 human embryonic fibroblasts. *RSC Adv.* **2019**, *9*, 26787–26798, doi:10.1039/c9ra03313k.

57. Samutprasert, P.; Chiablaem, K.; Teeraseranee, C.; Phaiyarin, P.; Pukfukdee, P.; Pienpinijtham, P.; Svasti, J.; Palaga, T.; Lirdprapamongkol, K.; Wanichwecharungruang, S. Epigallocatechin gallate-zinc oxide co-crystalline nanoparticles as an anticancer drug that is non-toxic to normal cells. *RSC Adv.* **2018**, *8*, 7369–7376, doi:10.1039/c7ra10997k.

58. Zhang, L.; Xie, J.; Gan, R.; Wu, Z.; Luo, H.; Chen, X.; Lu, Y.; Wu, L.; Zheng, D. Synergistic inhibition of lung cancer cells by EGCG and NF-κB inhibitor BAY11-7082. *J. Cancer* **2019**, *10*, 6543–6556, doi:10.7150/jca.34285.

59. Luo, K.W.; Lung, W.Y.; Chun-Xie; Luo, X. Le; Huang, W.R. EGCG inhibited bladder

cancer T24 and 5637 cell proliferation and migration via PI3K/AKT pathway. *Oncotarget* **2018**, *9*, 12261–12272, doi:10.18632/oncotarget.24301.